Applied Physics Letters

Magnetism and unconventional topology in $LaCoO_3/SrIrO_3$ heterostructure

Cite as: Appl. Phys. Lett. **122**, 021602 (2023); https://doi.org/10.1063/5.0113188
Submitted: 23 July 2022 • Accepted: 03 January 2023 • Published Online: 11 January 2023

Samir Rom, Santu Baidya, Subhro Bhattacharjee, et al.

Applied Physics Letters ARTICLE scitation.org/journal/apl

Magnetism and unconventional topology in $LaCoO_3/SrIrO_3$ heterostructure

Cite as: Appl. Phys. Lett. **122**, 021602 (2023); doi: 10.1063/5.0113188
Submitted: 23 July 2022 · Accepted: 3 January 2023 ·
Published Online: 11 January 2023

View Online Export Citation CrossMark

Samir Rom,[1] Santu Baidya,[2] Subhro Bhattacharjee,[3] and Tanusri Saha-Dasgupta[1,a)]

AFFILIATIONS

[1]S.N. Bose National Centre for Basic Sciences, JD Block, Sector III, Salt Lake, Kolkata 700106, India
[2]Materials Research Centre, Indian Institute of Science, Bangalore 560012, India
[3]International Centre for Theoretical Sciences, Tata Institute of Fundamental Research, Bangalore 560089, India

Note: This paper is part of the APL Special Collection on Metal Oxide Thin-Film Electronics.
[a)]**Author to whom correspondence should be addressed:** tanusri@bose.res.in

ABSTRACT

Employing first-principles calculations, we provide microscopic insights on the curious magnetic and topological properties of $LaCoO_3$/$SrIrO_3$ heterostructure, which has been recently synthesized [Kumar Jaiswal *et al.*, Adv. Mater. **34**, 2109163 (2022)]. Our computational study unravels transfer of polar charge from $SrIrO_3$ to $LaCoO_3$, thereby reducing the Co valence from 3+ toward 2+, supporting the experimental findings. Our study further reveals the stabilization of the intermediate spin state of Co and strong ferromagnetic Co–Co coupling in the $LaCoO_3$ block of the heterostructure. This, in turn, is found to induce ferromagnetism in the pseudo-tetragonally structured $SrIrO_3$ in the heterostructure geometry, providing an understanding of the origin of magnetism, which is counter-intuitive as both $LaCoO_3$ and $SrIrO_3$ are nonmagnetic in bulk form. Most interestingly, the band structure of ferromagnetic, tetragonal structured $SrIrO_3$ is found to exhibit unconventional topology, manifested as $C = 2$ double Weyl points, which leads to the observed anomalous Hall effect. Our finding of $C = 2$ double Weyl points, belonging to the class of charge-2 Dirac points, opens up the possibility of material realization of unconventional topological properties beyond the conventional Dirac and $C = 1$ Weyl points, which calls for future experiments.

Oxide heterostructures have drawn significant interest in recent times, due to the report of several emergent phenomena,[1–5] which can be observed at the interface (IF) between two perovskite oxides, though absent in their individual bulk forms.

Designing new heterostructures with improved physical properties, however, remains a challenging task. Recently, there has been a growing interest in 5d transition metal oxides (TMOs), which may show exciting quantum phenomena arising from the interplay of strong spin–orbit coupling (SOC) and electron–electron correlation. In particular, 5d iridium-based TMOs of Ruddlesden–Popper series $Sr_{n+1}Ir_nO_{3n+1}$ have received special attention.[6] Though the $n = 1$ member, Sr_2IrO_4 is a SOC driven magnetic insulator[7] with half-filled doublet $J_{eff} = 1/2$, though the $n = \infty$ member, $SrIrO_3$ (SIO) displays paramagnetic semimetallic behavior due to enhanced Ir 5d-O 2p covalency.[8] The presence of SOC makes SIO a Dirac-nodal line semimetal.[9] Theoretical calculations, however, indicate SIO is very close to magnetic instability.[10] This has led to a surge of activities focusing on SIO-based heterostructures by placing SIO in contact with magnetically active layers like $SrRuO_3$[11] or manganite.[12] Following this route, very recently, the heterostructure of SIO and $LaCoO_3$ (LCO) has been synthesized,[13] which has been found to show sizable anomalous Hall effect (AHE) and anomalous magnetoresistance. This finding, however, is surprising, as bulk LCO at low temperature is a diamagnetic insulator,[14] as opposed to the magnetic nature of $SrRuO_3$ or manganite, used in other SIO-based heterostructures. It is pertinent to note here that, in the experimental setup, the heterostructure is formed on the $SrTiO_3$ (STO) substrate. The substrate effect of STO enforces a pseudo-tetragonal symmetry of both SIO and LCO. Although the strained tetragonal structure of SIO supports a canted antiferromagnetic state,[15] the desired ferromagnetism (FM) in SIO happens only when brought in contact with LCO, highlighting the crucial role of LCO.[13] This calls for need of a thorough theoretical investigation to provide a detailed microscopic understanding.

In order to theoretically investigate the physical properties of LCO/SIO heterostructures, we consider $[(LCO)_{m.5}/(SIO)_{n.5}]$ heterostructures in superlattice geometry, where the IrO_2 layer of SIO is placed next to the LaO layer of LCO. The in-plane lattice constants of the heterostructure are fixed at 3.905 Å to mimic the substrate effect of

STO. Both SIO and LCO in the studied geometry are strained, SIO being compressed by ∼1.1% and LCO being expanded by ∼1.5%. Fixing the in-plane lattice constant, the out-of-plane lattice constant is relaxed, including the z-coordinate of the atoms. The calculations are carried out within the plane wave-based pseudopotential framework of density functional theory (DFT) as implemented in the Vienna *ab initio* Simulation Package.[16,17] The generalized gradient approximation (GGA) is chosen to describe the exchange-correlation functional. The effect of SOC, which is especially effective at the Ir sites, is considered through the GGA + SOC calculations. The effect of the strong electron–electron correlation effect at the TM sites of Co and Ir beyond GGA is supplemented through $+U$ calculations within the rotationally invariant formulation.[18] The U and J_H values at the Ir site are fixed at 2 and 0.5 eV, respectively, following the literature.[19] To further cross-check the literature value, constrained density functional theory calculations[20] are carried out for SIO. This resulted in U and J_H values of 2.2 and 0.45 eV, respectively, at the Ir site, close to the values chosen in the present calculations.

Bulk LCO is a much-discussed compound due to its temperature-induced spin state transition and its associated debate on the nature of the spin state. The choice of U and J_H values has been reported to have a strong influence on the calculated spin state of Co ion in the bulk $LaCoO_3$.[14] Thus, in the present calculations, U and J_H values on Co are varied over a wide range to check the influence of U and J_H. The other details of the method are presented in the supplementary material.

The top panel of Fig. 1 shows the schematic illustration of the studied $[(LCO)_{m.5}/(SIO)_{n.5}]$ superlattice structure with the in-plane lattice constants restricted to that of the STO substrate. It is to be noted that A+/B+ cations in SIO are in 2+/4+ valence states with neutral LaO and IrO_2 layers, while for LCO, it is in 3+/3+ valence states with positively charged LaO layer of +1 charge and negatively charged CoO_2 layer of −1 charge. Neutral IrO_2 layer of SIO facing positively charged LaO of LCO, therefore, creates an n-type interface (IF). We consider two symmetric n-type interfaces in the periodic cell of the superlattice geometry, which results in nonstoichiometric supercells with an additional IrO_2 layer in SIO and an additional LaO layer in LCO. n is chosen to be 4, and m is varied from 4 to 6. The trend in the structural, electronic, and magnetic properties is found to be the same between the three studied systems with $m = 4$, 5, and 6. Bottom panel of Fig. 1 shows the tilt of the CoO_6 and IrO_6 octahedra as well as the distortion of the octahedra, measured in terms of the metal–oxygen bond length variation, plotted as a function of the layer number. The layers are numbered from IF, with IF + l (IF − l) referring to the TM layers belonging to the SIO (LCO) block. As expected, the tilt and the distortion of the octahedra are found to be maximum at the IF, with values in IrO_6 (CoO_6) octahedra 15° (25°) and 0.2 (0.45) Å, respectively. Both the tilt and the bond distortion are found to progressively decrease as one moves toward the center of each block, tilt being vanishingly small at the center of the blocks.

A polar discontinuity happens at the IF, due to the creation of the heterostructure between the neutral layers of SIO and the charged layers of LCO. This creates a diverging electrostatic potential, which can be avoided by the interfacial polar charge transfer. The direction of the interfacial charge transfer is an important quantity influencing the properties of the heterostructure. Projection of the layer resolved density of states to Ir d states (presented in supplementary material) reveals that the Ir electronic structure exhibits negligible layer

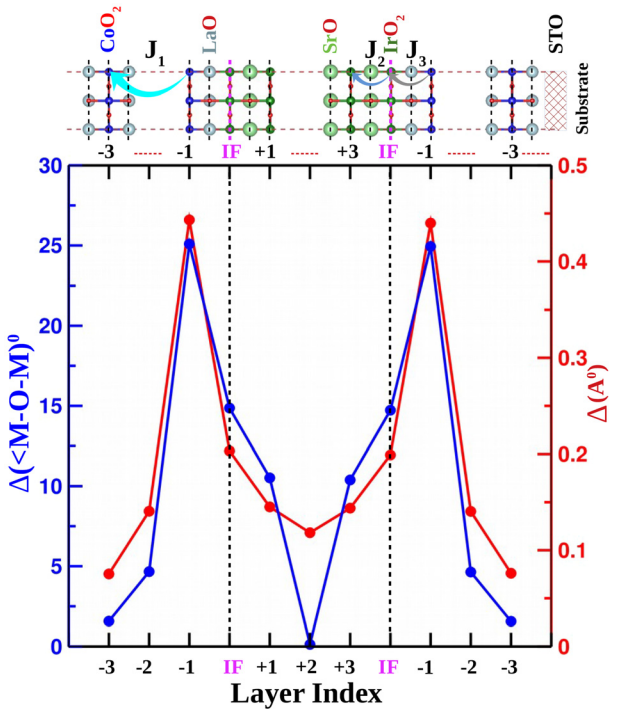

FIG. 1. Top: schematic representation of the SIO/LCO superlattice structure on a STO substrate. Marked are the n-type IF formed between the IrO_2 layer of SIO and the LaO layer of LCO, and the different TM-O layers, along with the magnetic exchanges, J_1, J_2, and J_3. Bottom: the distortion of the CoO_6 and IrO_6 octahedron plotted as a function of the layer index, for $m = 4$ superlattice. Distortion is measured in terms of the tilt angle, deviation of the TM–O–TM bond-angle from 180° (left axis), and the tetragonal bond distortion (right axis).

dependency. The crystal field split and the spin split Ir t_{2g} states strongly admixed with O p states and cross the Fermi level (E_F) with empty, e_g states. This makes SIO in the heterostructure geometry a ferromagnetic metal. This is supported by the calculated magnetic moment of ∼0.5 μ_B at Ir site that includes orbital moment of ∼0.1 μ_B. The magnetic moment at the O sites in the IrO_2 layer is found to be appreciable (∼0.1 μ_B). Focusing on the Co electronic structure, in the majority spin channel, the crystal field split Co t_{2g} states are fully occupied, while the very broad Co e_g states are partially filled crossing E_F with low density of states at E_F. In the minority spin channel, on the other hand, the Co e_g states are completely empty, with the Co t_{2g} states mostly filled with an unfilled part that gets gaped out from the filled part due to the combined effect of crystal field splitting and U. The low density of states at E_F in the majority spin channel may get localized by the disorder effect, presumably accounting for the experimental observation.[13] The Co d states, in contrast to the Ir d states, exhibit layer dependency; the electronic structure close to E_F of the Co atoms belonging to the layers close to the IF is different from those belonging to the layers distant from the IF. The partially filled part of the Co e_g states in the majority spin channel is found to be appreciably larger for the layer next to the IF, compared to those away from the IF. This is also reflected in the calculated magnetic moment, which shows a magnetic moment at the layers close to IF being ∼0.3 μ_B larger compared to that away from IF (cf. Fig. 2, top panel). This is also supported

by the Bader charge analysis,[21] which shows larger charge occupancy ($\sim$0.2 e^-) of the Co sites close to the IF compared to those away from the IF (cf. Fig. 2, bottom panel). We note that the calculated magnetic moments of the Co ions (including contribution from the oxygen atoms) are between 2 and 3μ_B, depending on the choice of U and J_H. In the fully polarized limit, the nominal Co^{3+} valence in $3d^6$ configuration can give to moment of 0, 2, and 4 μ_B in its low-spin (LS), intermediate-spin (IS), and high-spin (HS) states, respectively.[14] We, thus, conclude that the valence state of Co is reduced from 3+ in the bulk structure toward 2+ in the heterostructure. The Co valence is, thus, (3-δ)+, with δ being larger for the Co atoms in the layer adjacent to the IF, compared to those belonging to the layers away from the IF. The corresponding spin state is an IS state. In order to cross-check the possible dependency of the charge and the spin state of Co on the choice of Coulomb parameters, U and J_H, we repeated the calculations by varying the U value over a large range of 4–7 eV, and the J_H value over a range of 0.6–1.0 eV (shown in Fig. 2, top panel, for the representative cases). We find that, in all the cases, the calculated magnetic moments lie within 2–3 μ_B with larger moment at the layers adjacent to the IF compared to those away from the IF, establishing the robustness of our conclusion. This confirms the interfacial charge flow to

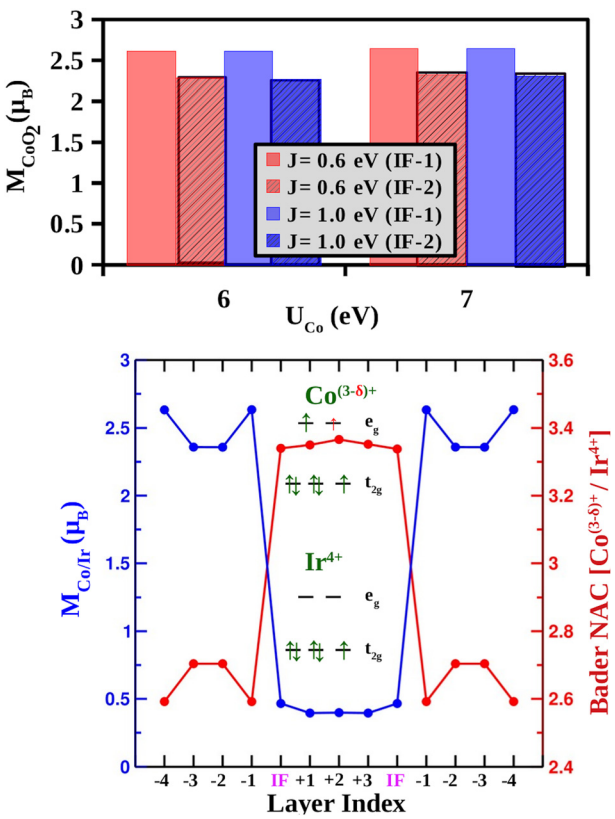

FIG. 2. Top: the computed magnetic moment at CoO_2 layers, adjacent to the IF, (IF-1) and next to that, (IF-2), for different choices of U and J_H values at the Co site. Bottom: the magnetic moment (left axis) and the Bader charge (right axis) at the Co and Ir sites, plotted as a function of the layer index, for the $m = 4$ LCO/SIO superlattice. Inset shows the electron occupancy of the Ir and the Co octahedrally crystal field split d levels.

LCO, which percolates from the IF to the LCO block. This is in perfect agreement with the experimental findings,[13] as inferred from energy loss spectroscopy. The stabilization of IS of Co, as found in the present study, calls for further experimental investigation.

To have an understanding of the magnetic ground state, in addition to the knowledge of the magnetic states of the transition metal ions in the system, as established above, the magnetic exchanges need to be investigated. As shown in Fig. 1, the primary magnetic interactions are the nearest neighbor (NN) Co–Co interaction in the LCO block, the Co–Ir interaction across the interface, and the Ir–Ir interaction in the SIO block. To estimate the above-mentioned three interactions, we consider five different spin arrangements with different possible alignments of Co and Ir spins (see the supplementary material). We find the computed total energy of each spin arrangement strongly depends on the structural relaxation of the atomic positions with the enforced magnetic structure. This indicates a strong magneto-structural coupling present in the heterostructure. Remarkably, the parallel alignment of the Co and Ir spins in the LCO and SIO block is favored among all the studied spin arrangements. Mapping the calculated total energies to a NN spin model, the estimated values of J_1, J_2, and J_3 turned out to be +8.8, +0.6, and +1.6 meV, respectively, where the positive sign signifies FM interaction. This highlights the fact that it is the strong FM in the LCO block, which induces FM in SIO through the Co–Ir magnetic interaction. The calculation for magneto-crystalline anisotropy shows a strong preference for in-plane orientation of spins with an energy gain of $\sim$4 meV/Ir-atom over the out-of-plane orientation, in agreement with experimental findings.[13]

As mentioned before, possible topological property of the bulk SIO has been investigated both theoretically and experimentally,[9,22] and its calculated band structure was found to possess a line node made of $J_{eff} = 1/2$ bands below the Fermi level.[9] Angle-resolved photoemission (ARPES) studies on strained SIO on STO or $(LaAlO_3)_{0.3}(Sr_2TaAlO_6)_{0.7}$ (LSAT) substrate found the signature of Dirac line nodes that were found to be gapped.[22] Experimental observation of large AHE[13] in LCO/SIO heterostructure points toward the interplay of magnetism and topology of SIO in contact with LCO. It is to be noted that the heterostructure geometry makes SIO ferromagnetic through the interfacial Co–Ir interaction, as discussed above, and imposes pseudo-tetragonal symmetry in contrast to paramagnetic, monoclinic symmetry of bulk SIO. The topological properties of FM and tetragonal SIO, thus, needed to be probed.

The top panel of Fig. 3 shows the GGA + SOC + U band structure of FM, tetragonal SIO, which confirms its metallic nature along with several band crossings around E_F. The tetragonal symmetry gives rise to the orbital degeneracy between d_{yz} and d_{xz} of the Ir t_{2g} manifold, and between p_x and p_y of the O p. In recent times, there has been a search for topological semimetals beyond the conventional Dirac and Weyl ones, which are characterized by higher topological charges. In this context, double Weyl point band crossings have been discussed.[23] They can be threefold degenerate spin-1 Weyl points with linear crossing of $C = 2$ and an extra flatband,[24] or fourfold degenerate charge-2 Dirac points,[23] which are direct sum of two identical spin-1/2 Weyl points,[25] or twofold degenerate charge-2 Weyl point with quadratic dispersion.[26]

The FM SIO with orbital degeneracy may open up the possibility of realizing such double Weyl points. Focusing on the band structure, close to the A point (π/a, π/a, π/c) along M(π/a, π/a, 0) − A − Z(0, 0, π/c), we find two linear crossings: one 0.01 eV above E_F and another 0.02 eV below E_F (see encircled parts in Fig. 3, bottom panels), apart

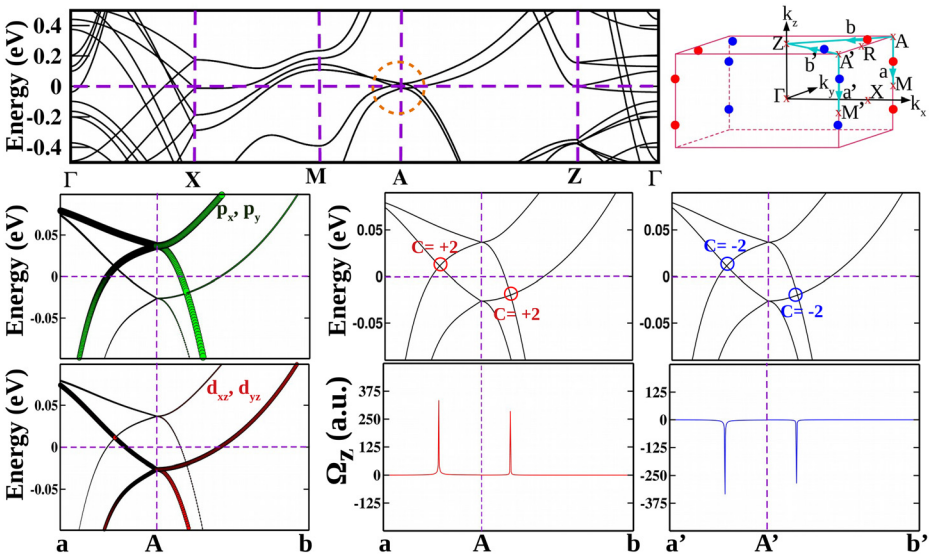

FIG. 3. Top: the GGA + SOC + U band structure of FM, tetragonal SIO, with in-plane lattice parameters constrained to that of STO (left), plotted along the high-symmetry directions of the tetragonal Brillouin zone (BZ) (right). Bottom: left—band structure, zoomed along $a = (\pi/a, \pi/a, 0.126\ \pi/c) - A = (\pi/a, \pi/a, \pi/c) - b = (0.224\ \pi/a, 0.224\ \pi/a, \pi/c)$, and the symmetry-related path, $a' = (\pi/a, -\pi/a, 0.126\ \pi/c) - A' = (\pi/a, -\pi/a, \pi/c) - b' = (0.224\ \pi/a, -0.224\ \pi/a, \pi/c)$, projected onto the Ir d_{xz}/d_{yz} and the O p_x/p_y orbitals. Middle—calculated Chern numbers and Berry curvatures of the two crossings above and below E_F along a–A–b. Right—the same along a′–A′–b′. See the top, right panel for the positioning of a, a′, b, and b′ in the BZ, with Weyl points of positive and negative chirality, colored as red and blue, respectively.

from two symmetry-allowed semi-Dirac crossings at high-symmetry A (A′) point. The crossing arises due to the intersection of two doubly degenerate pairs of bands, originating from degenerate Ir d_{xz}/d_{yz} and O p_x/p_y orbitals, as shown in the two bottoms, left panels of Fig. 3.

Turning to these linear crossings away from high-symmetry A point, the degenerate orbitals transform into each other under symmetries and lead to two degenerate Weyl points occurring at the same momenta, **K**. These linear crossings can be described by the low energy Hamiltonian $\mathscr{H} = H \otimes \sigma_0$, where H is the Hamiltonian for each Weyl point and σ_0 is the identity in the orbital space. This leads to double Weyl points that are locally stable if there is no mixing with the Weyl point of opposite chirality or lifting orbital degeneracy, which are characterized by a topological charge of $C = \pm 2$, thus fulfilling the requirement of a charge-2 Dirac point.

Indeed, the calculated Chern number of the crossing at $\mathbf{K} = (\pi/a, \pi/a, 0.339)$ above E_F turned to be $+2$, while that at the symmetry-related crossing at $\mathbf{K} = (\pi/a, -\pi/a, 0.339)$ turned to be -2. Similarly, the calculated Chern number of the crossing at $\mathbf{K} = (0.446\ \pi/a, 0.446\ 0.446\pi/a, \pi/a)$ above E_F turned to be $+2$, while that at the symmetry-related crossing at $\mathbf{K} = (0.446\ \pi/a, -0.446\ \pi/a, \pi/a)$ turned to be -2, as shown in the bottom, middle, and bottom, right panels of Fig. 3. The opposite chiralities of Weyl points above and below E_F, away from the high-symmetry A points, are further confirmed by the opposite signs of calculated Berry curvatures (cf. Fig. 3). The calculated intrinsic anomalous Hall conductivity (AHC), originating from the Berry curvature effect, turned out to be positive and strong, with a value of $7.5\,\Omega^{-1}\,\mathrm{cm}^{-1}$, in good agreement with the measured value.[13] An adaptively refined[27] k-grid of $16 \times 16 \times 16$ is found to be sufficient to give the converged value of AHC.

In conclusion, our first-principles study on $LaCoO_3/SrIrO_3$ heterostructure provides a microscopic understanding of the counter-intuitive ferromagnetism in the system and unravels its curious topological properties. Our study confirms the experimental observation of interfacial charge flow to the $LaCoO_3$ block, thereby reducing the nominal valence of Co from 3+ toward 2+. Our study further makes a prediction of the IS state of Co, generating strong ferromagnetic exchanges between the Co sites, although in the ground state of bulk LCO, Co stabilizes in the diamagnetic LS state. The strong Co–Co ferromagnetic exchange is found to induce the ferromagnetic long-range order in the SIO block through interfacial Co–Ir magnetic interaction. This clarifies the role of LCO in the stabilization of magnetism in the LCO/SIO heterostructure. The ferromagnetic, tetragonal structured SIO, constrained to STO substrate, is found to host charge-2 Dirac points, driven by the orbital degeneracy. This not only provides microscopic understanding of the observed AHE in LCO/SIO heterostructure[13] but most importantly also opens up the door for materials realization of novel quasiparticles beyond the known Dirac and Weyl points.

See the supplementary material for the density of states plot, Hubbard parameter dependency of magnetic moments, details of calculation of magnetic exchanges, and details of the method.

T.S.-D. acknowledges J. C. Bose National Fellowship (Grant No. JCB/2020/000004) for funding. S.Bh. acknowledges funding from the Max Planck Partner Group Grant at ICTS, Swarna Jayanti fellowship grant of SERB-DST (India), under Grant No. SB/SJF/2021-22/12 and the Department of Atomic Energy, Government of India, under Project No. RTI4001. T.S.-D. and S.B. would like to thank Vajra (Grant No. SERB/F/373/2022023) for the collaboration. The authors thank Saumya Mukherjee for bringing the problem into our notice and valuable discussions.

AUTHOR DECLARATIONS

Conflict of Interest

The authors have no conflicts to disclose.

Author Contributions

Samir Rom: Data curation (lead); Methodology (equal); Software (equal). **Santu Baidya:** Methodology (supporting). **Subhro Bhattacharjee:**

Methodology (supporting). **Tanusri Saha-Dasgupta:** Conceptualization (lead).

DATA AVAILABILITY

The data that support the findings of this study are available from the corresponding author upon reasonable request.

REFERENCES

[1]R. Ramesh and V. G. Keramidas, Annu. Rev. Mater. Sci. **25**, 647 (1995).
[2]Z. Huang, Ariando, X. R. Wang, A. Rusydi, J. Chen, H. Yang, and T. Venkatesan, Adv. Mater. **30**, 1802439 (2018).
[3]A. Ohtomo and H. Hwang, Nature **427**, 423 (2004).
[4]Y.-L. Han, S.-C. Shen, J. You, H.-O. Li, Z.-Z. Luo, C.-J. Li, G.-L. Qu, C.-M. Xiong, R.-F. Dou, L. He, D. Naugle, G.-P. Guo, and J.-C. Nie, Appl. Phys. Lett. **105**, 192603 (2014).
[5]M. Y. Zhuravlev, R. F. Sabirianov, S. Jaswal, and E. Y. Tsymbal, Phys. Rev. Lett. **94**, 246802 (2005).
[6]W. Witczak-Krempa, G. Chen, Y. B. Kim, and L. Balents, Ann. Rev. Condens. Matter Phys. **5**, 57 (2014).
[7]B. J. Kim, H. Jin, S. J. Moon, J.-Y. Kim, B.-G. Park, C. S. Leem, J. Yu, T. W. Noh, C. Kim, S.-J. Oh *et al.*, Phys. Rev. Lett. **101**, 076402 (2008).
[8]Z. T. Liu, M. Y. Li, Q. F. Li, J. S. Liu, W. Li, H. F. Yang, Q. Yao, C. C. Fan, X. G. Wan, Z. Wang, and D. W. Shen, Sci. Rep. **6**, 30309 (2016).
[9]M. Ahsan Zeb and H.-Y. Kee, Phys. Rev. B **86**, 085149 (2012).
[10]J.-M. Carter, V. V. Shankar, M. A. Zeb, and H.-Y. Kee, Phys. Rev. B **85**, 115105 (2012).
[11]J. Matsuno, N. Ogawa, K. Yasuda, F. Kagawa, W. Koshibae, N. Nagaosa, Y. Tokura, and M. Kawasaki, Sci. Adv. **2**, e1600304 (2021).
[12]G. A. Ovsyannikov, T. A. Shaikhulov, K. L. Stankevich, Y. Khaydukov, and N. V. Andreev, Phys. Rev. B **102**, 144401 (2020).
[13]A. Kumar Jaiswal, D. Wang, V. Wollersen, R. Schneider, M. Le Tacon, and D. Fuchs, Adv. Mater. **34**, 2109163 (2022).
[14]M. A. Korotin, S. Y. Ezhov, I. V. Solovyev, V. I. Anisimov, D. I. Khomskii, and G. A. Sawatzky, Phys. Rev. B **54**, 5309 (1996).
[15]T. R. Dasa, L. Hao, J. Yang, J. Liu, and H. Xu, Mater. Today Phys. **4**, 43 (2018).
[16]G. Kresse and J. Hafner, Phys. Rev. B **47**, 558 (1993).
[17]G. Kresse and J. Furthmüller, Phys. Rev. B **54**, 11169 (1996).
[18]A. I. Liechtenstein, V. I. Anisimov, and J. Zaanen, Phys. Rev. B **52**, R5467 (1995).
[19]T. R. Dasa, L. Hao, J. Liu, and H. Xu, J. Mater. Chem. C **7**, 13294 (2019).
[20]V. I. Anisimov and O. Gunnarsson, Phys. Rev. B **43**, 7570 (1991); P. H. Dederichs, S. Blügel, R. Zeller, and H. Akai, Phys. Rev. Lett. **53**, 2512 (1984).
[21]E. Sanville, S. D. Kenny, R. Smith, and G. Henkelman, J. Comput. Chem. **28**, 899 (2007).
[22]Y. F. Nie, P. D. C. King, C. H. Kim, M. Uchida, H. I. Wei, B. D. Faeth, J. P. Ruf, J. P. C. Ruff, L. Xie, X. Pan, C. J. Fennie, D. G. Schlom, and K. M. Shen, Phys. Rev. Lett. **114**, 016401 (2015).
[23]T. Zhang, Z. Song, A. Alexandradinata, H. Weng, C. Fang, L. Lu, and Z. Fang, Phys. Rev. Lett. **120**, 016401 (2018).
[24]B. Bradlyn, J. Cano, Z. Wang, M. G. Vergniory, C. Felser, R. J. Cava, and B. A. Bernevig, Science **353**, aaf5037 (2016).
[25]Z. Rao, H. Li, T. Zhang *et al.*, Nature **567**, 496 (2019).
[26]H. He, C. Qiu, X. Cai, M. Xiao, M. Ke, F. Zhang, and Z. Liu, Nat. Commun. **11**, 1820 (2020).
[27]Y. Yao, L. Kleinman, A. H. MacDonald, J. Sinova, T. Jungwirth, D. S. Wang, E. Wang, and Q. Niu, Phys. Rev. Lett. **92**, 037204 (2004).